CHAPTER 7

STRUCTURAL TRANSFORMATION IN Au-Cu NANOPARTICLES

This chapter deals with structural transformations in Au-Cu nanoparticles observed after heat treatment in solution phase. They have been investigated through extensive usage of TEM. Results obtained are discussed critically in relation to information available in literature. Conclusions from this part of the investigations are given at the end.

7.1 Introduction

The control of external shapes and size of the elemental and disordered / ordered bimetallic NPs are critical for their uses in various applications [63, 124, 223, 253–259]. Understanding of the nature of structural transformations in nanocrystalline solids is equally important as they are novel to nanometer length scale. Such structural features influence properties. Wet-chemical route of syntheses currently serves as the most versatile approach for the formation of alloy NPs. Alloy NPs containing noble metals displaying ordering are the most active area of investigations [93–96, 253, 257, 260, 261]. Some of the pioneering efforts in this direction pertain to investigations by Sra and co-workers [62, 64, 262]. In one of the methods they began with Au and Cu nanoparticle precursors in appropriate proportion. These precursors were heat treated in the temperature range of 200 - 400 ^{o}C for obtaining ordered cubic $AuCu_3$ (cP4) and tetragonal AuCu (tP4) phases. They are found in the equilibrium phase diagram in these temperature ranges [80]. The

phase diagram of Au-Cu is complex in nature with appearence of several intermetallics such as Au_3 Cu, AuCu and $AuCu_3$ at lower temperatures (below 400^{o}C). Further, presence of dotted lines in the equilibrium phase diagram around this temperature range suggest formation of many intermetallic phases in the phase field that needs to be explored further. In addition to that, alloying behaviour of Au-Cu at lower temperature during wet chemical synthesis of nanoparticles is under initial stage. The growth of substrate supported clusters with Au_3Cu, AuCu, and $AuCu_3$ stoichiometry have been studied extensively [196]. The Au_3 Cu, AuCu and $AuCu_3$ ordered phases have been observed through chemical syntheses albeit at relatively lower temperature than that of their bulk counterparts [62, 94, 96, 253, 257]. This opened up an avenue to explore the alternative solution syntheses routes. Seed-mediated growth in particular has been used for the synthesis of various types of bimetallic nanocrystals [63, 94, 124, 253, 255]. Polyol based syntheses have received greater attention among other methods owing to their well-known chemistry involved in the process [124, 223, 256, 260]. The mechanisms of transformation seem to be poorly understood despite extensive investigations on Au-Cu ordered phases. The complexity introduced at nanoscale poses newer challenges. Nanomaterials syntheses have been shown to yield new phases owing to defects inherent during synthesis at nanoscale. This chapter of the thesis explores some of the above mentioned challenges.

7.2 Experimental details

The synthesis of Au-Cu nanoparticles was carried out by modified polyol method in a single pot. The desired product was achieved in three steps. In the first step, $HAuCl_4.3H_2O$

was mixed in oleylamine and oleic acid mixture. This mixture was taken in a 15 mL borosilicate glass vial and placed in a silicone oil bath at around 90^oC for uniform heating for dissolution. It was bubbled with Argon gas for about 15 min. The temperature of the oil bath was further raised to $\sim 120^oC$. The vibrant yellow colour disappears (indicator of Au^{3+} to Au^{+}) followed light pink colour appears indicating reduction of Au^{+} to Au^{0}. This serves as seed. In the second step, $CuCl_2.2H_2O$ precursor solution according to desired stoichiometry was mixed in the Au-seed dispersion and oil bath temperature was raised to 180^oC. It was kept for about 1 h to promote diffusion of Cu in the Au seed. In the third step, the oil bath temperature was further raised to $\sim 290^oC$ and the reaction vial kept there for 2 h. This was followed by cooling it to room temperature. The product was collected by cleaning with toluene and ethanol at least three times and finally dispersed in hexane for its further characterization. It may be pointed out that green colour supernatant was observed after centrifugation. This was indicative of the fact that all the amount of $CuCl_2.2H_2O$ did not take part in the process of reaction. Aliquots were taken out after heating at 180 ^oC for 1h and 290^oC for 2 h. This was done to understand the growth sequence during the process of synthesis. A drop of the suspension was dispersed on carbon coated Ni grid. The morphology and structure of the synthesized Au-Cu nanoparticles was investigated with TEM (FEI Tecnai G^2 T20 operating at 200 kV). The chemical analysis of these samples was studied by HAADF-STEM- EDS. In order to get the structural information by single particle, nano beam diffraction (NBD) was captured. The exposure time of CCD camera was kept at $\sim$ 2 s for recording NBD patterns to minimize the drift. High resolution phase contrast images were acquired to understand the underlying

structural details of the ordered Au-Cu nanoparticles.

7.3 Results and discussion

Figure 7.1 (a) shows the bright field TEM image and corresponding SAD pattern of AuCu nanoparticles synthesized at 180 ^{o}C for 1h (cf. Figure 7.1 (b)).

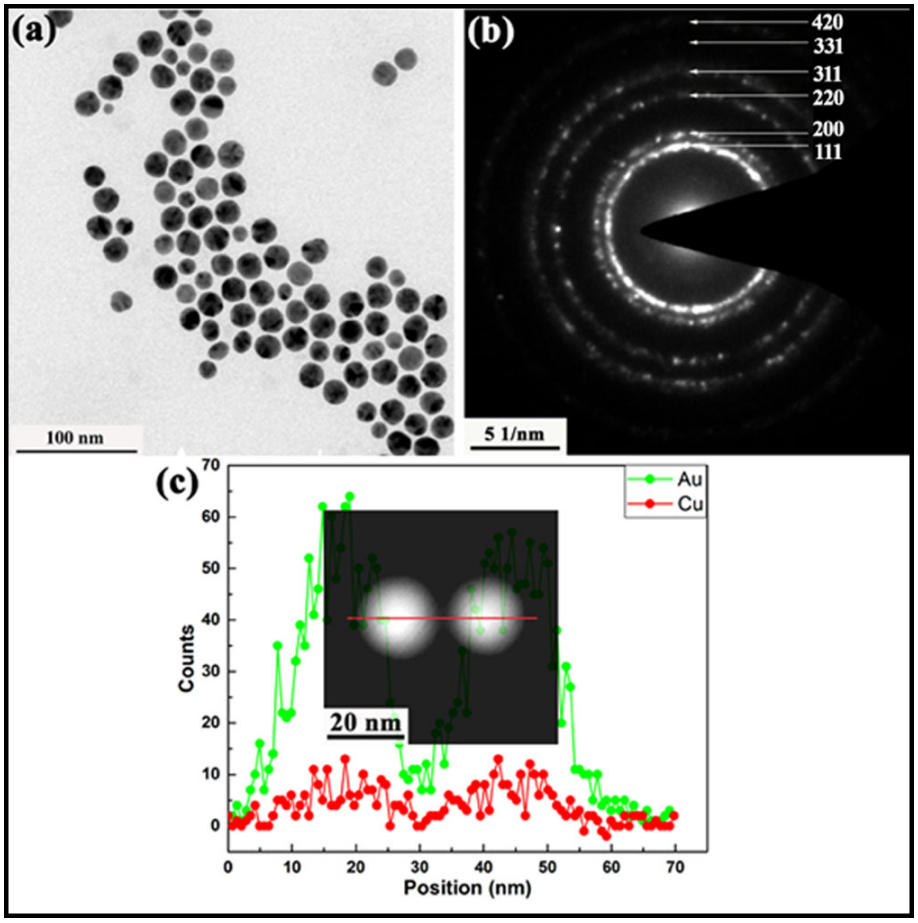

FIGURE 7.1: Bright field TEM image (a), corresponding selected area diffraction pattern (b) and STEM-EDS line scan across two particle (c) of the Au-Cu alloy nanoparticles sample reacted at 180 ^{o}C for 1 h.

The Au and Cu elemental line scan of two such AuCu nanoparticles (shown in green and red colour respectively) acquired by STEM-EDS is depicted in Figure 7.1

(c). The nearly spherical morphology of the formed AuCu nanoparticles was observed as seen in Figure 7.1(a). The ring pattern obtained in SAD mode was indexed as shown in Figure 7.1 (b) and structure was found to be FCC. The measured spacing of the rings corresponding to {111}, {200}, {220}, and {311} were found at 2.31 Å, 2.00 Å, 1 .42 Å, and 1.19 Å respectively. These d-values are smaller than that of standard FCC-Au reflections and lattice parameter was estimated to be $\sim$ 3.99 Å. Moreover, reflections

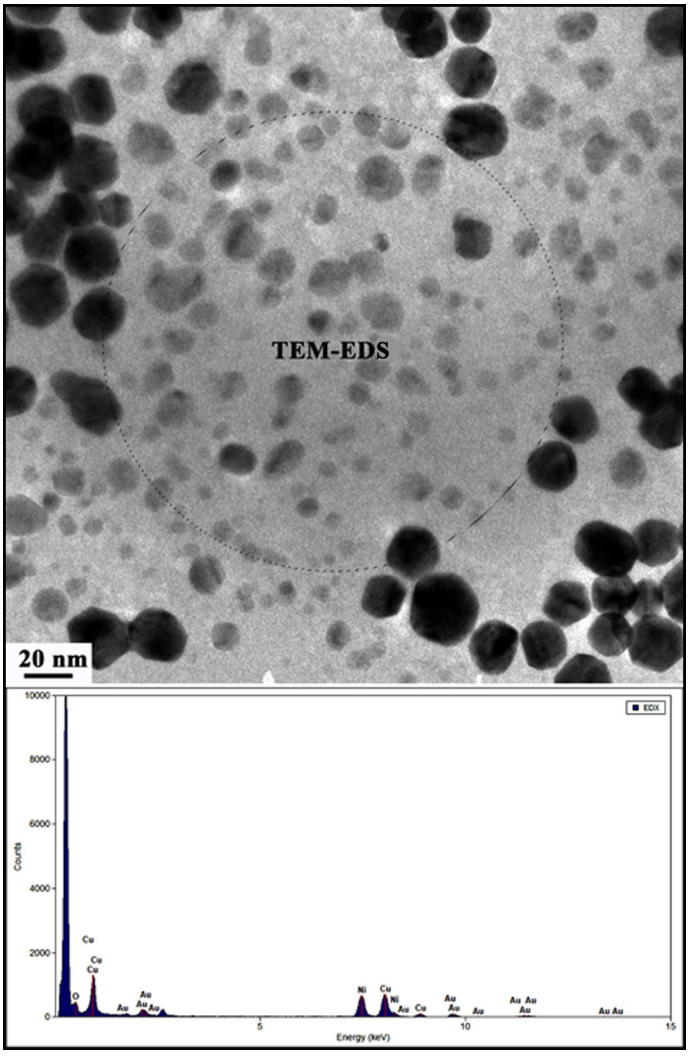

FIGURE 7.2: TEM image showing AuCu nanoparticles heat treated at 290 ^{o}C for 2 h and TEM-EDS spectrum corresponding to selected area encircled in the image.

corresponding to FCC-Cu in the SAD pattern were not observed. The reduction in d-values compared to standard FCC-Au and absence of Cu reflections indicate the formation of a single phase solid solution of Cu in Au. The average elemental composition of Au and Cu in the AuCu nanoparticles was found to be $\sim$ 80 atom % and $\sim$ 20 atom % respectively as quantified with TEM-EDS results. The lattice parameter derived from Vegard's law for this composition was $\sim$ 3.98 Å. The Au and Cu elemental line profiles across two AuCu nanoparticles show the homogeneous distribution of Au and Cu in the particles and confirm the formation of a single phase of AuCu alloy nanoparticles (Figure 7.1 (c)). The representative TEM image and corresponding SAD pattern of AuCu nanoparticles processed at 290^{o}C for 2 h is presented in Figure 7.3 (a) and (b) respectively. The Au and Cu elemental line scan across such a particle obtained by STEM-EDS is shown in Figure 7.3 (c). The morphology observed in this case is faceted unlike the AuCu nanoparticles processed at 180 ^{o}C. The polycrystalline diffraction pattern show additional rings along with those observed in Figure 7.1 (b). These extra reflections correspond to ordered cubic $AuCu_3$ (a = 3.75 Å) (cP4) and tetragonal AuCu (a = 3.98 Å; c=3.72 Å) (tP4) phases. For instance, reflections $\{100\}$, $\{110\}$, $\{211\}$ of former and $\{210\}$ of the latter are shown in Figure 7.3 (b). The average elemental composition of Au and Cu in nanoparticles was found to be 57 atom % and 43 atom % respectively. This has been arrived at based on TEM / STEM-EDS analyses carried out at least at ten different locations each covering at least 100 nanoparticles given in Table 7.1. The presence of Cu-rich regions was also observed which compensate the Cu stoichiometry in the synthesis (cf. Figure 7.2).

The composition of Cu therefore has increased substantially from 20 atom %

to 43 atom % owing to heat treatment at 290^{o}C for 2 h. The unreacted Cu precursor seems to have reduced along with promoting diffusion of reduced Cu atoms into already present Au-Cu bimetallic nanoparticles. The deviation of Au and Cu in the alloy nanoparticle is within 3 atom %. The line scan across one of the particles depicts uniform distribution of Au and Cu within the particle (cf. Figure 7.3 (c)). The Au and Cu elemental maps using STEM-HAADF-EDS from an ensemble of particles is given in Figure 7.4.

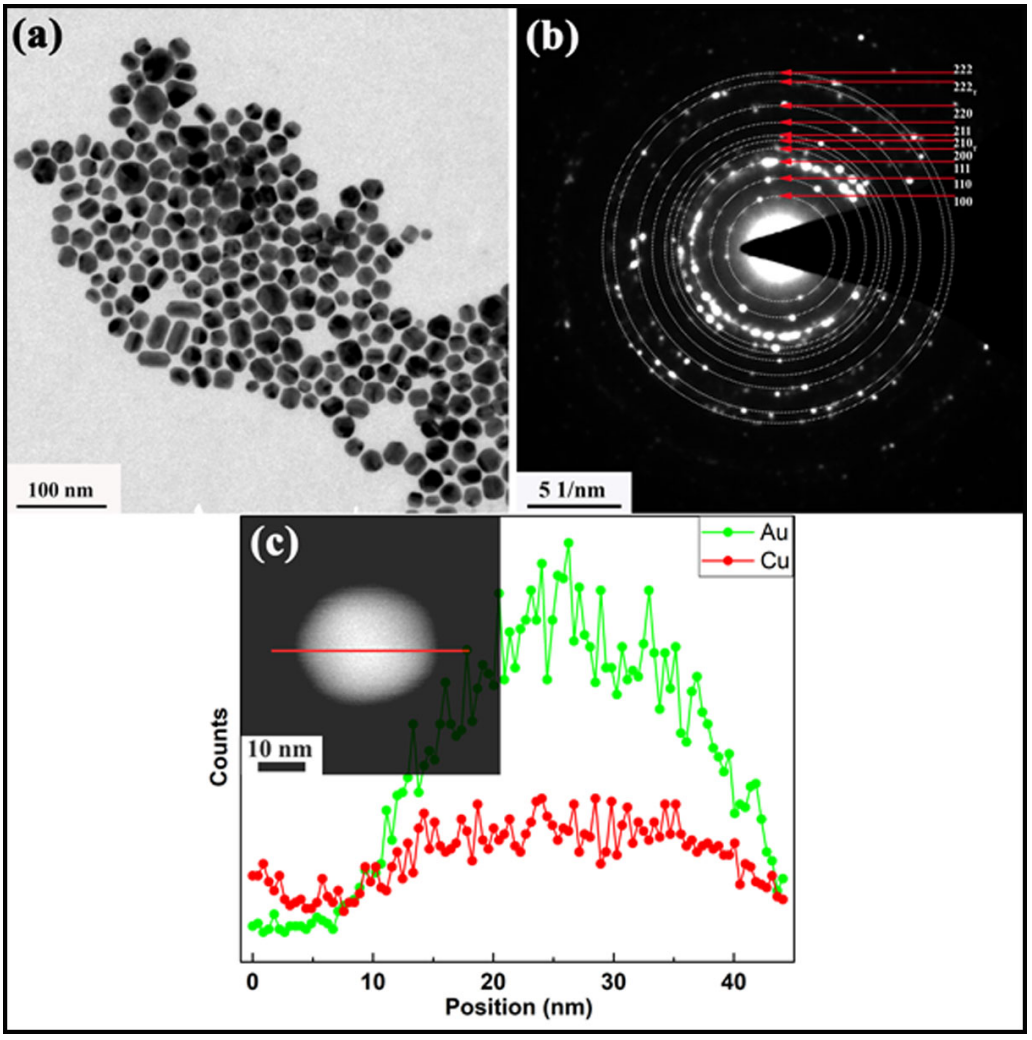

FIGURE 7.3: BF TEM image (a), corresponding SAD pattern (b), and STEM-EDS line scan of a single nanoparticle for Au-Cu nanoparticles processed at 290^{o}C for 2 h. The schematic rings (white color) are inserted in SAD pattern to show the disposition of reflections.

The technique of NBD was thought to be important for deciphering structural features in a chosen particle. While making extensive investigation of individual nanoparticles with the help of NBD, many new structural characteristics have been observed.They will be discussed below.

The NBD pattern acquired from a single particle and corresponding computer generated electron diffraction patterns are shown in Figures 7.5 (a) and (b) respectively. Stacked stereographic plots with orientation relationship are depicted in Figure 7.5 (c). Figure 7.5 (d) displays HRTEM image of such a particle together with lattice fringe spacing and FFT pattern of the selected region (shown as dotted white colour square). This NBD pattern could be indexed with split zone scheme with ordered cubic AuCu phase having lattice parameter (a $\sim$ 3.98 Å). The reflections corresponding to two zones are schematized as red and dotted white nets in the Figure 7.5 (a). The patterns corresponding to red and white nets were indexed based on $[1\bar{1}0]$ and $[1\bar{1}1]]$ zone axes of an ordered tetragonal AuCu respectively having metrical property akin to that of a cube. Figure 7.5 (b) shows the suitably superimposed diffraction patterns computed separately

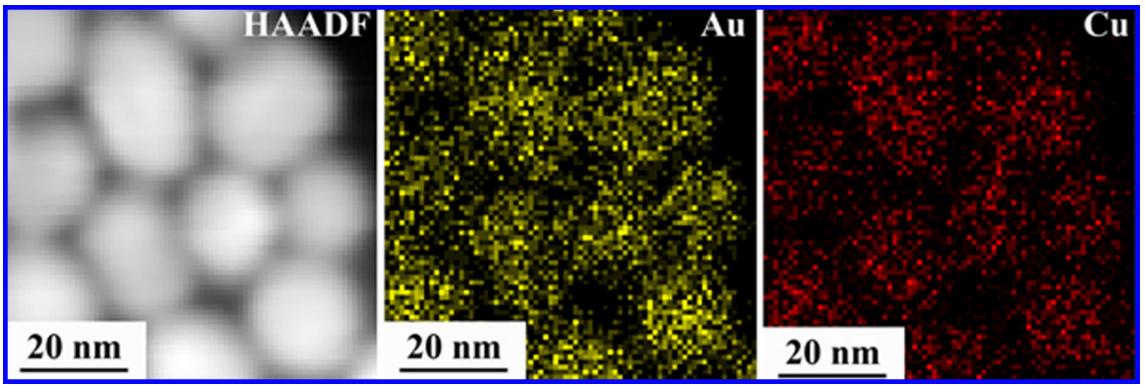

FIGURE 7.4: STEM-HAADF-EDS elemental mapping of AuCu nanoparticles processed at 290 ^{o}C for 2 h.

along[$1\bar{1}0$]and [$1\bar{1}1$] zones. The computed pattern matches well with the experimentally obtained NBD pattern. The orientation relationships of the two crystals are found to be AuCu [$1\bar{1}0$] //AuCu [$1\bar{1}1$] ; AuCu(110) //AuCu(110). This is corroborated by stacked stereographic projection plot (cf. Figure 7.5 (c)) of cubic AuCu with above mentioned

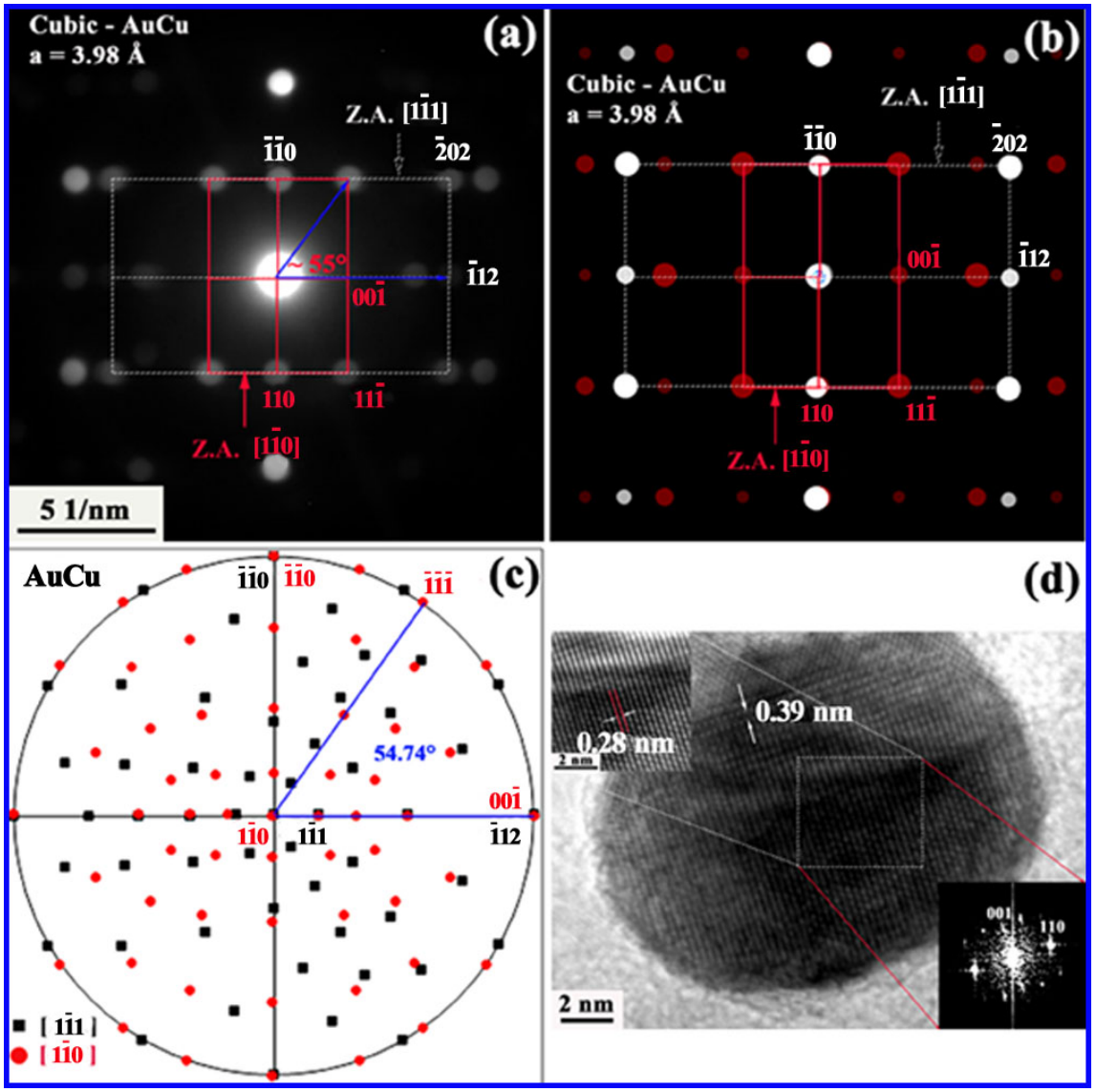

FIGURE 7.5: Experimental nano beam diffraction from a single particle (a), computer generated electron diffraction pattern (b), stacked stereographic plots along [$1\bar{1}0$]and [$1\bar{1}1$] directions (c) maintaining orientation relationship in conformity with (a), and high resolution TEM micrograph with FFT (bottom right) and background corrected image (top left) as insets (d).

orientation relationship, projected from $[1\bar{1}0]$ and $[1\bar{1}1]$ zones and matching it with experimental NBD pattern. The superimposed diffraction patterns are computed based on Au occupancy at (0, 0, 0) and (1/2,1/2,0) whereas Cu is occupying position at (1/2,0,1/2) and (0,1/2,1/2). As a consequence of this one sees one 4-fold axis along [001] cubic axis. The absence of 3-fold is also noted in the computed diffraction pattern along $[1\bar{1}1]$] for this cell. The computed diffraction patterns along [010] and [100] display only two fold symmetry. Thus, it has been concluded that the chemical ordering of the classical ordered tetragonal AuCu cell (a = 3.98Å, c = 3.72 Å) leads to metrical properties akin to that of a cube whereas symmetry remains conforming to that of a tetragonal cell.Such a cell will be referred to as pseudo cubic cell. Such a situation may arise through partial substitution of Au on Cu site in a statistical manner. The HRTEM image revealed lattice fringe spacing of 0.39 nm and 0.28 nm (indicated in the micrograph) corresponding to $\{001\}$ and $\{110\}$ planes of transformed pseudo cubic AuCu phase (Figure 7.5 (d)). The FFT also revealed $\{001\}$ and $\{110\}$ reflections of such a phase. A HRTEM image displaying above mentioned orientation relationship is shown in Figure 7.6.

The NBD pattern acquired from another set of single particle and corresponding computer generated diffraction patterns are shown in Figures 7.7 (a) and (b) respectively. This NBD pattern could be indexed by superimposition of ordered cubic $AuCu_3$ phase (a $\sim$ 3.75 Å) along$[1\bar{2}1]$ zone (green net) and cubic $AuCu_3$ phase with (a $\sim$ 3.5 Å) along [010] zone (red net). The two different cubic phases will be referred to as $AuCu_3$ [I] and $AuCu_3$ [II] from here onwards. The electron diffraction patterns of phases $AuCu_3$ [I] along $[1\bar{2}1]$ and $AuCu_3$ [II] along [010] zones were computed separately and

superimposed to get the pattern as shown in Figure 7.7 (b). The orientation relationship between two different phases was found to be $AuCu_3$ [I] [$1\bar{2}1$]]//$AuCu_3$ [II] [010];$AuCu_3$ [I](111)//$AuCu_3$ [II]($\bar{1}$ 01). The stacked stereographic projection plot having above orientation relationship is depicted in Figure 7.7 (c). The angular relationship between diffracted spots $(210)_I$ and $(001)_{II}$ in this Figure is noted to be $\sim 5\ ^o$. This is also observed in experimental NBD pattern in Figure 7.7 (a). They are encircled to indicate these in the respective Figures. In addition to this, satellite reflections were observed along [111] of $AuCu_3$ [I] phase in NBD pattern. The reciprocal vector corresponding to this fundamental reflection is divided into five equal parts. This leads to symmetry breaking of the basic cubic $AuCu_3$ [I]. Thus, the repeat along [111] is $\sim$ 11Å in real space which is approximately five times of d_{111} of $AuCu_3$ [I]. One also notes that this spacing is equal to

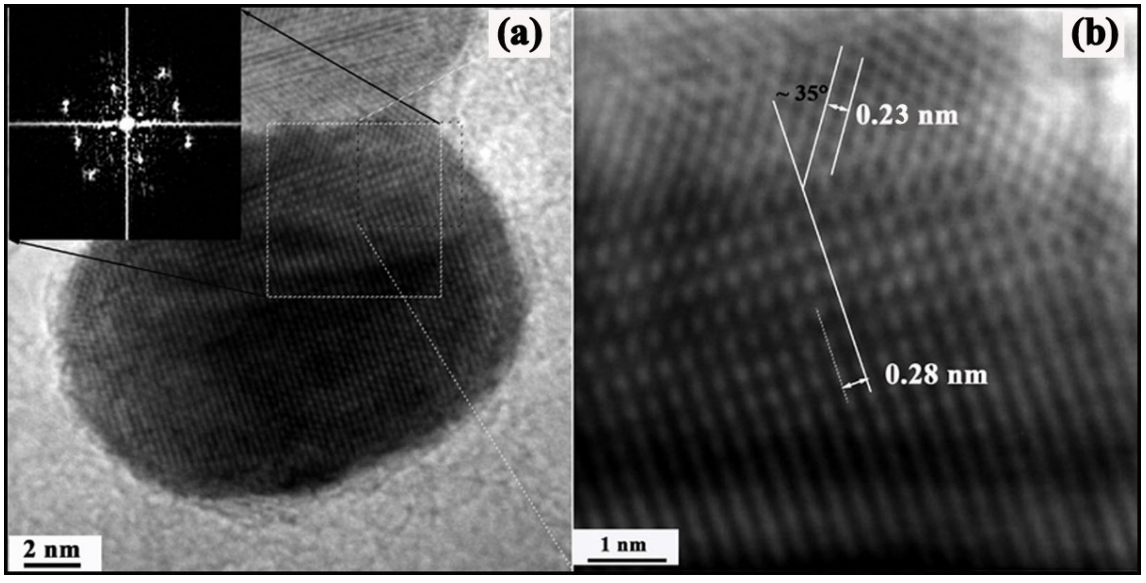

FIGURE 7.6: HRTEM micrograph showing transformed cubic AuCu crystals having orientation relationship AuCu [$1\bar{1}0$]//AuCu [$1\bar{1}1$]];AuCu(110)//AuCu(110) (a).The inset in Figure (a) shows FFT corresponding to selected region and is similar to NBD pattern. The magnified image depicts two domains of the crystals having $\{110\}$ planes making an angle of $\sim 35^0$ (b).

three times of d_{001} of cubic $AuCu_3$ [II]. The HRTEM micrograph acquired from the same particle shows lattice fringes with spacing $\sim$ 11 Å corresponding to measured spacing in NBD. The particle displays two inter grown crystals. One of them refers to bigger cell

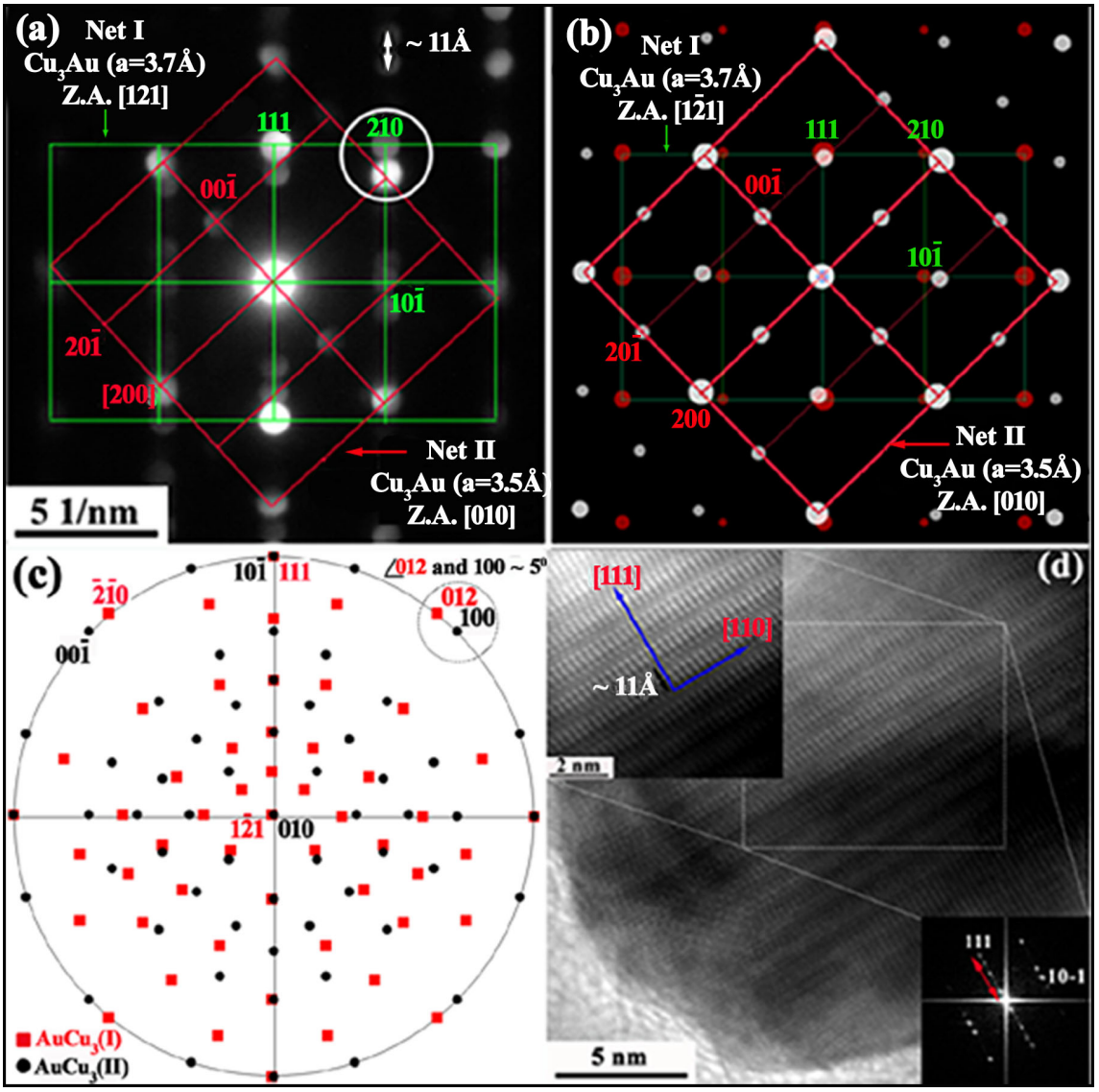

FIGURE 7.7: Experimental nano beam diffraction pattern (a), computer generated electron diffraction pattern (not to the scale) (b), stereographic projection plot projected along [1$\bar{2}$1]and [1$\bar{1}$1] zones (encircled poles from two zones) (c), and HRTEM micrograph with FFT (arrow displaying division of 111 reflection into 5 parts) and background corrected image (arrow showing real space distance $\sim$ 11 Å along [111] direction) as insets (d).

size ($AuCu_3$[I]) accompanied with ordering along [111] direction. The other displays lattice fringes along [001] of reduced cell size ($AuCu_3$ [II]). They can be seen in Figure 7.8. The FFT in the inset (bottom right) of Figure 7.7 (d) shows similar distribution of satellite reflections along [111] direction. The repeat of the fringes as displayed in the background corrected image (shown in the inset of Figure 7.7 (d) on top left) also reveals spacing $\sim$ 11Å. Thus, repeat distance along [111] seen in NBD and HRTEM conform to each other. It is important therefore to explain such an observation. It has been reported in literature that such ordering takes place in Al-Cu-Ni system along $<$ 111 $>$ directions owing to vacancy ordering on the (Cu + Ni) site of a fundamental cubic cell [263, 264]. When such an ordering is invoked in our case then it will be shown that both the crystallographic features that are new in AuCu system can be understood on uniform footing. It is noted

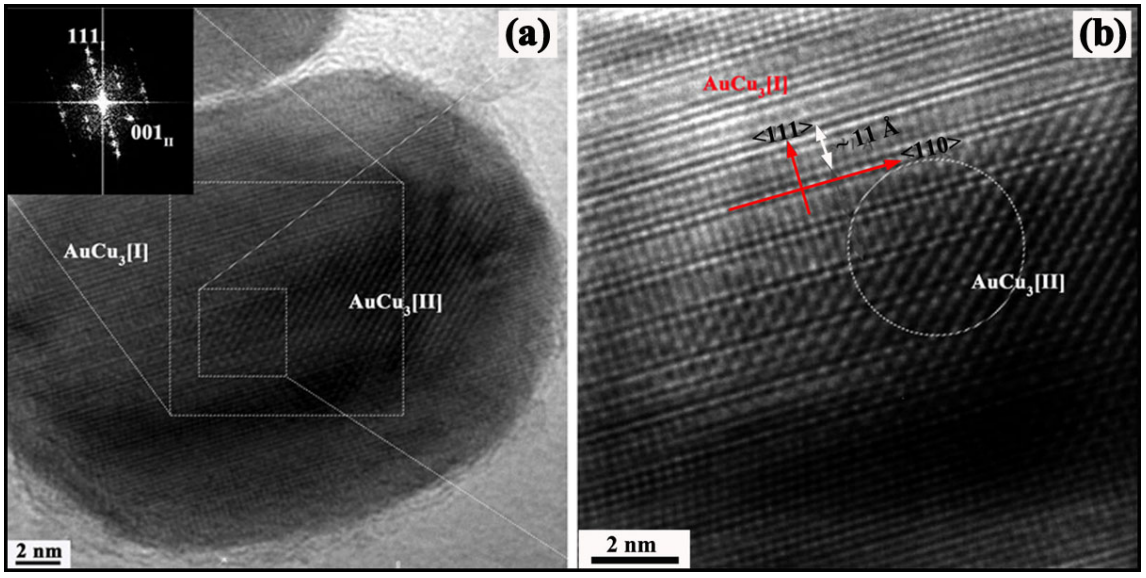

FIGURE 7.8: HRTEM micrograph depict coexisting cubic AuCu3 [I] and AuCu3 [II] phases having orientation relationship $AuCu_3$ [I] [$1\bar{2}1$]]//$AuCu_3$ [II] [010];$AuCu_3$ [I](111)//$AuCu_3$ [II]($\bar{1}$01). The inset in Figure (a) shows FFT corresponding to selected region and is similar to NBD pattern. The two cubic phases are displayed in the magnified HRTEM image (b). The spacing $\sim$ 11 Å along [111] direction is also shown. The interfered region of the two phases is encircled.

TABLE 7.1: Elemental composition of Au and Cu in atom % in AuCu nanoparticles processed at 180 ^{o}C for 1 h and 290 ^{o}C for 2 h acquired from TEM/STEM-EDS analyses.

AuCu Nanoparticles: 180 ^{o}C for 1 h			**AuCu Nanoparticles: 290 ^{o}C for 2 h**		
Sl. No.	**Au (atom %)**	**Cu (atom%)**	**Sl. No.**	**Au (atom%)**	**Cu (atom%)**
1	82	18	1	68	32
2	83	17	2	60	40
3	80	20	3	43	57
4	81	19	4	62	38
5	77	23	5	68	32
6	83	17	6	69	31
7	80	20	7	64	36
8	81	19	**STEM-EDS**		
9	81	19	8	84	16
10	84	16	9	57	43
Average	**$\sim$81 atom%**	**$\sim$19 atom%**	10	65	35
Composition from single particle (AuCu NPs: 290^{o}C for 2 h)			11	55	45
1	46	54	12	63	37
2	41	59	13	55	45
3	50	50	14	45	55
4	60	40	15	68	32
5	47	53	16	45	55
-	-	-	17	58	42
-	-	-	18	65	35
-	-	-	19	43	57
-	-	-	20	34	66
-	-	-	21	53	47
-	-	-	22	68	32
Average	**$\sim$49 atom%**	**$\sim$51 atom%**	**Average**	**$\sim$57 atom%**	**$\sim$43 atom%**

that Au has got a cell size of $\sim$ 4.08 Å and that of Cu is $\sim$ 3.61 Å. All the ordered phases reported in this system conform to lattice parameter a = 3.75 Å for $AuCu_3$ whereas a = b = 3.98 Å and c = 3.72 Å for AuCu tetragonal phase. All these are lying between the lattice parameters corresponding to Au and Cu FCC structures. As mentioned previously, existence of $AuCu_3$ [II] having cubic cell parameter $\sim$ 3.5 Å in this investigation that is less than even that of Cu FCC cell. One of the ways to understand such a decrease in cell

size is to think of statistical occupancy of vacancy on Cu site. Such an ordering will lead to decrease in the average cell size of the well-known cubic phase $AuCu_3$. In contrast to this, ordering on Cu site in this cell with vacancy may lead to increase in the repeat along [111] direction. Such an ordering in literature is known as commensurate ordering [265]. The AuCu system is known to display long period superstructure [197, 198, 266, 267]. These observation illustrate an example of such superstructure owing to commensurate ordering of vacancy on Cu site. It has been further noted that such a commensuration leaves only one of the 3-folds of the basic cubic cell leading to a new ordered cell having trigonal symmetry. The mechanisms of formation of these phases seem to be mediated by vacancy in this investigation. Hence, one may expect coexistence of these phases in the same nanoparticle. This can be corroborated through observations in NBD as well as in the HRTEM image. Vacancies in NPs are expected to contribute to the diffusion rearrangement leading to the formation of the diverse internal structure. As a consequence, structural phase transformations may be observed inside NPs. This needs to be understood before considering them suitable for applications. It is important to point out here that Cu atoms at face centred positions may not retain hard sphere model necessary for metallic bonds. As a consequence of this, intermetallic phase $AuCu_3$ [II] may have less metallicity in the $\{111\}$ plane and shape will be oval for Cu [268]. This should be the case even for cP4 $AuCu_3$ structure as $[2r_{FCC(Cu)}+2r_{FCC(Au)}]$ along face diagonal is greater than that of $\sqrt{2}\times3.75$Å , where $r_{FCC(Cu)}$ (radius of Cu atom)= 1.27Å and $r_{FCC(Au)}$ (radius of Au atom)= 1.44Å. The trigonal cell of $AuCu_3$ [I] type may be understood by recalling the stacking sequence along $< 111 >$ direction of the cP4 structure. This will be

.....ABCABCA.....with a difference that the layer may not have fully metallic character unlike solid solution phases. Also, these layers are having occupancies of Au and Cu atoms. Vacancy may be changing chemistry of these layers owing to its occupancy at Cu site as stated above. In addition to this, deletion of a layer at regular interval may break the symmetry of the cubic phase. For example a stacking sequence along any one of the $< 111 >$ direction after a systematic deletion of a layer of the type .....ABC V BCABC V BCA..... may have 5 layers of repeat along this ("V" stands for vacancy). Such a repeat will concurrently lead to retention of a 3-fold along this, leading to transformation to a trigonal one. This may be the reason for the formation of $AuCu_3$ [I] trigonal cell. Afore-said two phases $AuCu_3$ [I] and $AuCu_3$ [II] are normally seen to be coexisting together. As a consequence of this, chemistry of these phases could not be ascertained with the help of available microscopic facility.

7.4 Conclusions

The formation of three new phases by heat treatment of Au-Cu NPs at $\sim 290\ ^{o}$C in solution phase have been established. One of them relates to modification of the AuCu tetragonal cell (tP4) mimicking cubic cell characteristics without losing tetragonal symmetry. The other two relates to vacancy ordering along $< 111 >$ directions based on an ordered $AuCu_3$ cubic phase (cP4). On one hand, statistical occupancy of vacancy on Cu site in $\{111\}$ planes lead to the reduction of cell size from $\sim$ 3.75 Å to $\sim$ 3.5 Å whereas introduction of a vacant layer on the other hand, gives rise to symmetry breaking leading to formation of a trigonal cell.